Nonmonotonic quantum-to-classical transition in multiparticle interference

Young-Sik Ra[a], Malte C. Tichy[b,c], Hyang-Tag Lim[a], Osung Kwon[a], Florian Mintert[b,d], Andreas Buchleitner[b], and Yoon-Ho Kim[a,1]

[a]Department of Physics, Pohang University of Science and Technology, Pohang 790-784, Korea; [b]Physikalisches Institut and [d]Freiburg Institute for Advanced Studies, Albert-Ludwigs-Universität, D-79104 Freiburg, Germany; and [c]Lundbeck Foundation Theoretical Center for Quantum System Research, Department of Physics and Astronomy, University of Aarhus, DK–8000 Aarhus C, Denmark

Edited by Alain Aspect, Institut d'Optique, Orsay, France, and approved December 10, 2012 (received for review April 24, 2012)

Quantum-mechanical wave–particle duality implies that probability distributions for granular detection events exhibit wave-like interference. On the single-particle level, this leads to self-interference—e.g., on transit across a double slit—for photons as well as for large, massive particles, provided that no which-way information is available to any observer, even in principle. When more than one particle enters the game, their specific many-particle quantum features are manifested in correlation functions, provided the particles cannot be distinguished. We are used to believe that interference fades away monotonically with increasing distinguishability—in accord with available experimental evidence on the single- and on the many-particle level. Here, we demonstrate experimentally and theoretically that such monotonicity of the quantum-to-classical transition is the exception rather than the rule whenever more than two particles interfere. As the distinguishability of the particles is continuously increased, different numbers of particles effectively interfere, which leads to interference signals that are, in general, nonmonotonic functions of the distinguishability of the particles. This observation opens perspectives for the experimental characterization of many-particle coherence and sheds light on decoherence processes in many-particle systems.

quantum interference | which-path information | quantum statistics

The double-slit-like (self-)interference of single particles has been observed for particles ranging from photons (1) to massive particles (2). It relies on the coherence of the single-particle wave-function, which guarantees that the different pathways a particle can take to a detector—e.g., through the left or through the right slit in a double-slit experiment—remain indistinguishable.

Interaction with the environment, however, may convey which-path information to the environment, and then inevitably leads to decoherence (3, 4). Thereby, it jeopardizes the ideal interference pattern and induces the quantum-to-classical transition (5, 6). The stronger the decoherence, the weaker is the interference signal (3). Expectation values of observables therefore depend monotonically on the strength of decoherence, and a monotonic transition between quantum and classical expectation values takes place (2, 5–10).

The superposition principle, which is responsible for the above self-interference effects, also applies to many-particle wave-functions, with entanglement (11) and many-particle interference (12) as immediate consequences. For the observation of the latter, the mutual indistinguishability of the particles is necessary and it entails, for instance, the Hong–Ou–Mandel (HOM) effect (13, 14): When a single photon is incident on each of the two input modes of a balanced beam splitter (BS), the two-particle Feynman paths of "both photons reflected" and "both photons transmitted" interfere destructively, leading to the strict suppression of the event with one particle per output mode.

As particles turn distinguishable, e.g., in a dynamical process, the ideal multiparticle interference is degraded (13, 15). This is because information available on the identity of the interfering particles provides which-path information, now in the space of many-particle paths, and, on this level, induces decoherence leading to the quantum-to-classical transition. In the HOM setting, the interference-induced suppression of the balanced output event fades away monotonically with increasing particle distinguishability (13, 16). Such monotonic distinguishability dependence of bunching events (where all particles are detected in one output mode) was also observed for four (17) and six (18) photons, whereas events other than bunching were not considered yet for more than two photons.

In our present contribution, we focus on many-particle interference effects in multiport output events distinct from bunching. In contrast to the hitherto-established scenario of the quantum-to-classical transition, we will see that the distinguishability-induced suppression of multiparticle interference signals is, in general, a nonmonotonic function of the indistinguishability of the particles, provided that more than two particles interfere (19). This will be explained by a hierarchy of interferences of different numbers of particles, which dominate the total interference signal at different stages of the distinguishability transition. Only when reduced indistinguishability defines two unambiguous alternatives does one enter the monotonic realm of the quantum-to-classical transition.

We establish this general scenario by considering photons that impinge on the input modes of a balanced (50:50) BS, as sketched in Fig. 1*A*. The quantum-to-classical transition is implemented by controlling the distinguishability of ancillary temporal degrees of freedom of photons (20, 21). The path delay x controls the difference of the arrival times of photons in the modes a and b, resulting in a continuous change of their (in-)distinguishability. The distinguishability of two photons with different arrival times t_1 and t_2 is quantified by the following:

$$|\alpha|^2 = \exp\left(-\Delta\omega^2(t_2-t_1)^2/2\right), \qquad [1]$$

where $t_2 - t_1 = x/c$, c is the speed of light in vacuum, and each photon has a Gaussian frequency width $\Delta\omega$ (*Materials and Methods*). Increasing the arrival time difference $t_2 - t_1$ causes the gradual growth of the distinguishability, without inducing any phase variations, in contrast to other experiments reported in refs. 22 and 23. The photons are strictly indistinguishable for $|\alpha|^2 = 1$, and fully distinguishable for $|\alpha|^2 = 0$. For intermediate values of $|\alpha|^2$, Gram–Schmidt orthonormalization (*Materials and Methods*) (19) allows to rewrite a two-photon state with one photon in each input mode and arrival times t_1 and t_2, respectively, as follows:

Author contributions: Y.-S.R., M.C.T., F.M., A.B., and Y.-H.K. designed research; Y.-S.R., H.-T.L., and O.K. performed research; Y.-S.R., H.-T.L., and Y.-H.K. analyzed data; and Y.-S.R., M.C.T., A.B., and Y.-H.K. wrote the paper.

The authors declare no conflict of interest.

This article is a PNAS Direct Submission.

[1]To whom correspondence should be addressed. E-mail: yoonho72@gmail.com.

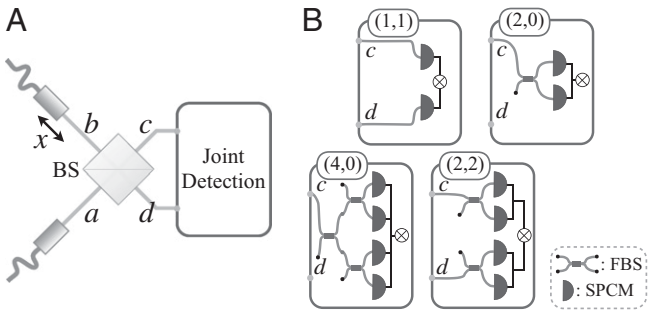

Fig. 1. Experimental setup. (*A*) HOM-type interferometer. The path delay *x* controls the distinguishability between the photons from mode *a* and *b*, which then scatter on the 50:50 BS. (*B*) Joint detection of (*m, n*) photons at the output modes *c* and *d*, to define a (*m, n*)-event. This is realized by concatenating fiber beam splitters (FBSs) (50:50) and single-photon counting modules (SPCMs).

$$a_{t_1}^{\dagger}\, b_{t_2}^{\dagger}|0\rangle = \alpha|1,1\rangle_{ab} + \sqrt{1-\alpha^2}|1,\tilde{1}\rangle_{ab}. \qquad [2]$$

The symbols $|1\rangle$ and $|\tilde{1}\rangle$ denote two different single-photon states, identified by their positions on the time axis (*Materials and Methods*). By construction, the state $|1\rangle$ is orthogonal to $|\tilde{1}\rangle$, such that these two basis states can be perceived as analogs of horizontal and vertical polarization. In the amplitude $|1,1\rangle_{ab}$, therefore, the two single photons cannot be distinguished through their arrival times and, consequently, interfere. In the amplitude $|1,\tilde{1}\rangle_{ab}$, however, the two single photons can be distinguished perfectly, hence do not interfere, in perfect analogy to photons with orthogonal polarization (24). The continuous parametrization of the distinguishability transition by x (Fig. 1*A* and Eq. **1**) is now replaced by $|\alpha|^2 \in [0;1]$. Only the indistinguishable component in Eq. **2** defines indistinguishable two-particle paths that can interfere, and the resulting interference signal therefore fades away monotonically with decreasing $|\alpha|^2$ (13).

Something qualitatively new happens when more than one photon is injected in each input mode: The orthogonal decomposition analogous to Eq. **2** gives rise to cross terms between the distinguishable and the indistinguishable components. Specifically, for two photons injected into each mode, we obtain the following:

$$\frac{1}{2}\left(a_{t_1}^{\dagger}\right)^2\left(b_{t_2}^{\dagger}\right)^2|0\rangle = \alpha^2|2,2\rangle_{ab} + \sqrt{2}\alpha\sqrt{1-\alpha^2}|2,1\tilde{1}\rangle_{ab} + \left(1-\alpha^2\right)|2,\tilde{2}\rangle_{ab}, \qquad [3]$$

with the cross term $\propto|2,1\tilde{1}\rangle_{ab}$ mutually orthogonal to $|2,2\rangle_{ab}$ and $|2,\tilde{2}\rangle_{ab}$. In precise analogy to the HOM scenario, the $|2,2\rangle_{ab}$ component defines indistinguishable four-particle paths that give rise to an interference signal with amplitude α^2, fading away with increasing amplitude $(1-\alpha^2)$ of the (distinguishable) $|2,\tilde{2}\rangle_{ab}$ component. In contrast, the cross term $\propto|2,1\tilde{1}\rangle_{ab}$ represents relative timing such that one of the two photons in mode *b* is strictly indistinguishable from those in mode *a*, whereas the other one is fully distinguishable. Therefore, this term gives rise to a three-particle interference signal through coherent superposition of indistinguishable three-particle paths, with amplitude $\sqrt{2}\alpha\sqrt{1-\alpha^2}$.

In general, when $N/2$ particles enter at each input mode, the event probability for detecting m particles in output mode *c* and n particles in output mode *d*, defined as an (m,n)-event, is given by the following:

$$P^{(N;m,n)}(x) = \sum_{\text{type}} p_{\text{type}}^{(N;m,n)}\; W_{\text{type}}^{(N)}(x), \qquad [4]$$

where we need to sum over the various "distinguishability types" of the contributions as they emerge in Eqs. **2** and **3** (19, 25): strictly indistinguishable (indis), fully distinguishable (dist), and—only for $N \geq 4$—partially distinguishable (inter). The associated detection probabilities $p_{\text{type}}^{(N;m,n)}$ for the different distinguishability types are determined by the geometry of the experimental setup (25, 26), computed by mapping input on output modes via the following:

$$a^{\dagger} \to \frac{1}{\sqrt{2}}\left(c^{\dagger} + d^{\dagger}\right),\;\; b^{\dagger} \to \frac{1}{\sqrt{2}}\left(c^{\dagger} - d^{\dagger}\right), \qquad [5]$$

and listed in Table 1 for the events (1, 1) and (2, 0) (for $N = 2$), and (2, 2) and (4, 0) (for $N = 4$).

The weights $W_{\text{type}}^{(N)}(x)$ in Eq. **4** are simply given by squaring the amplitudes of the respective components in the orthogonal decompositions in Eqs. **2** and **3**, respectively, where we denote the cross term $\propto|2,1\tilde{1}\rangle_{ab}$ by the label "inter." Their functional dependence on x, derived from their dependence on α via Eq. **1**, is shown in Fig. 2: although the weight of all particles being either strictly indistinguishable, $W_{\text{indis}}^{(2/4)}(x)$, or fully distinguishable, $W_{\text{dist}}^{(2/4)}(x)$, always depends monotonically on x, the weight $W_{\text{inter}}^{(4)}(x)$ representing cross terms between distinguishable and indistinguishable components exhibits a nonmonotonic x dependence! Consequently, in a four-particle experiment, three-particle interference contributions kick in while four-particle interference fades away, within a certain range of x. For the event (2, 2), we expect a nonmonotonic interference signal, because it is more strongly suppressed for the intermediate case than for strictly indistinguishable or fully distinguishable particles, as expressed by the relation $p_{\text{indis}}^{(4;2,2)} > p_{\text{inter}}^{(4;2,2)}$ and $p_{\text{inter}}^{(4;2,2)} < p_{\text{dist}}^{(4;2,2)}$ in Table 1.

We verify this prediction with an experimental implementation of the setup shown in Fig. 1*A*, for two and four photons. At the input modes *a* and *b*, a multiphoton quantum state generated via spontaneous parametric downconversion is injected. By postselection (*Materials and Methods*), exclusively the single-photon or two-photon Fock state components at the input modes, i.e., $|1,1\rangle_{ab}$ or $|2,2\rangle_{ab}$, are examined. Gradual increase of the path delay x of the mode *b* induces the quantum-to-classical transition, where the coherence length of the photons, $l_c = 134$ μm, defines the length scale over which the transition between strictly distinguishable ($\alpha = 0, x \gg l_c$) and indistinguishable photons ($\alpha \sim 1$, $x \ll l_c$) occurs. At each path delay x, m and n photons in the output modes *c* and *d* are monitored, respectively. See *Materials and Methods* for experimental details.

Table 1. Detection probabilities depending on distinguishability types and detection events

$p^{(N;m,n)}$	Indis	Inter	Dist
$N = 2$			
(2, 0)	1/2	—	1/4
(1, 1)	0	—	1/2
$N = 4$			
(4, 0)	3/8	3/16	1/16
(2, 2)	1/4	1/8	3/8

Detection probabilities $p^{(N;m,n)}$ of (m, n) particles in mode *c* and *d* are listed, depending on the distinguishability types strictly indistinguishable (Indis), partially distinguishable (Inter), and fully distinguishable (Dist), as they appear in Eqs. **2** and **3**, for $N = 2$ and $N = 4$.

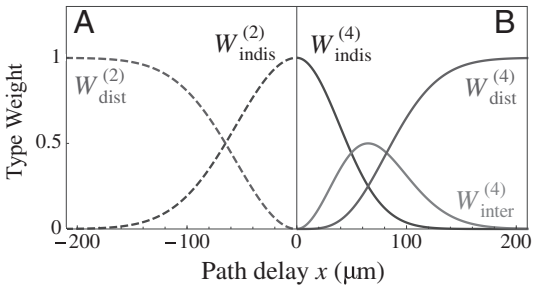

Fig. 2. Weights of contributions from different distinguishability types. Strictly indistinguishable [$W^{(N)}_{\rm indis}$], partially distinguishable [$W^{(N)}_{\rm inter}$], and fully distinguishable [$W^{(N)}_{\rm dist}$] particles contribute with different weights for each path delay x, which continuously parametrizes the distinguishability of the particles. (*A*) For $N = 2$, partial distinguishability does not arise, and $W^{(N)}_{\rm indis}$ and $W^{(N)}_{\rm dist}$ are monotonic functions of x, leading to a monotonic transition in $P^{(2;m,n)}(x)$. (*B*) In contrast, for $N = 4$, $W^{(N)}_{\rm inter}$ contributes nonmonotonically to the event probability, and induces the nonmonotonic behavior observed in Fig. 3*C*.

In a first step, we study the effect of the distinguishability transition for two photons. For variable x, we measured the probabilities of the two-photon events (1, 1) and (2, 0). The resulting data in Fig. 3*A* show typical two-photon HOM-type interferences (13, 27). As expected (13), the event probabilities are complementary and depend monotonically on the distinguishability of the photons. Next, the four-photon events, (4, 0) and (2, 2), are recorded, and we monitor the resulting four-photon distinguishability transition. A clear enhancement of (4, 0) events for indistinguishable photons is observed in Fig. 3*B*, and, indeed, this enhancement fades away monotonically as the photons are tuned to become distinguishable by increasing x. The event (2, 2), however, in Fig. 3*C*, exhibits minima symmetrically displaced from the origin $x = 0$, and the distinguishability transition is not any longer unambiguously reflected by a monotonic x dependence of the many-particle interference signal.

In Fig. 3, we compare all recorded data with the event probabilities given by Eq. **4**, using the $W^{(2/4)}_{\rm type}(x)$ in Fig. 2, together with the detection probabilities from Table 1. The theoretical prediction fits the experimental data perfectly well, without adjustable parameters besides the overall count rate. Note that bunching signals, as the (4, 0) event observed here, always exhibit a monotonic transition, as a consequence of the bosonic enhancement (28) of the associated, unique many-particle path, which induces the strict hierarchy $p^{(4;4,0)}_{\rm indis} > p^{(4;4,0)}_{\rm inter} > p^{(4;4,0)}_{\rm dist}$ in Table 1. We stress that the encountered nonmonotonicity in the (2, 2) event is fundamentally distinct from oscillating signals originating from single-photon interference in refs. 22 and 23. Also, it is not an effect of alternate two-photon interference contributions that kick in for different values of x in refs. 16 and 29. Rather, it presents a consequence of the changing weights of several superposed many-particle interference contributions (with different particle numbers involved) and constitutes an effect exclusive to setups with four or more particles that interfere simultaneously. Thus, this nonmonotonicity in the quantum-to-classical transition is an unprecedented and hitherto-unpredicted effect rooted in the intricate structure of multiparticle interference. It both contrasts and enriches previously reported monotonic behavior (2, 5–10, 13, 15–18).

In general, for $N/2$ particles per input mode, there are $N/2 - 1$ cross terms of distinguishable and indistinguishable components [represented by the term $\propto W^{(N)}_{\rm inter}(x)$ in Eq. **4**], which all depend nonmonotonically on x, and this nonmonotonicity is generically inherited by the derived event probabilities $P^{(N;m,n)}(x)$ [provided that it not be counterbalanced by the actual values of the detection probabilities $p^{(N;m,n)}_{\rm indis/inter/dist}$]. Fig. 4 shows an example for $N = 6$.

Let us finally discuss how this generic nonmonotonicity of many-particle interference signals in correlation functions such as $P^{(N;m,n)}(x)$ with respect to x matches our intuition of the monotonicity of the quantum-to-classical transition under decoherence (3): To begin with, the latter is generally observed in the interference of indistinguishable single-particle paths at one detector, whereas genuine many-particle interference manifests itself in multiparticle correlation functions not accessible in single-particle experiments. On this level, the distinguishability transition—possibly caused by environment interaction, i.e., coupling to additional degrees of freedom—reduces the order of many-particle interferences, e.g., from six- to five- and four-particle, or from four- to three-particle interference, in the examples considered in Figs. 2–4. As a consequence of the nonmonotonic dependence of the different orders of the many-particle interference contributions on the mutual distinguishability of the particles, the transition from fully many-particle multipath to single-particle coherence is, in general, nonmonotonic and, yet, fully consistent with our understanding of single-particle decoherence and the quantum-to-classical transition. The impact of the various interference contributions on measurable signals, described by Eq. **4**, allows the distinguishing of different orders of many-particle interference, which, in turn, may permit the characterization of different types of system–environment interaction [e.g., two- vs. three- or many-particle interactions (30)]. Reciprocally, the dependence of the

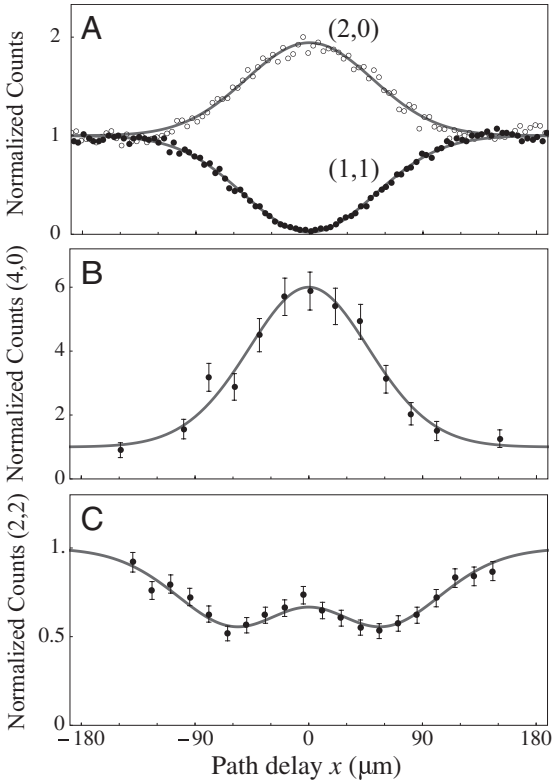

Fig. 3. Event probabilities versus path delay x. All coincidence counts are normalized to the coincidence counts at $x \gg l_c$, e.g., the background level. (*A*) HOM-type interference of two photons, with a clear enhancement of the (2, 0) event (open circles), and the corresponding suppression of the (1, 1) event (filled circles). Four-photon interference with two photons per input mode is shown in *B* for the (4, 0) event detection and in *C* for the (2, 2) event detection. The solid lines are the event probabilities as predicted by Eq. **4**, and they are in perfect agreement with the experimental data within the statistical error. Note that nonmonotonicity is clearly observed in *C*. The error bars represent 1 SD. In *A*, the error bars are smaller than the experimental data points due to high twofold detection rates.

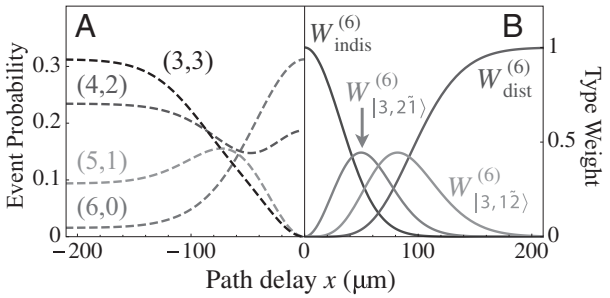

Fig. 4. Event probabilities and weights of distinguishability types in six-particle interference. (*A*) Event probabilities $P^{(N;m,n)}(x)$ are plotted for $N = m + n = 6$, and $m = 3,\ldots, 6$, for each three photons injected into modes *a* and *b* (Fig. 1*A*). The (4, 2) and (5, 1) events exhibit nonmonotonic transition. (*B*) The associated weights of strictly indistinguishable, partially and fully distinguishable contributions $W^{(N)}_{\text{indis/inter/dist}}$ with a notation strictly analogous to that introduced in Eq. **3** are plotted. Much as in Fig. 2*B*, the partially distinguishable contributions' weights are nonmonotonic in *x*.

various interference terms in Eq. **4** on the environment coupling parameters may serve as an analytic tool to distinguish distinct environment coupling mechanisms.

In conclusion, we studied theoretically and experimentally the transition between quantum and classical many-particle behavior, and we encountered a generic, nonmonotonic dependence of coincidence event probabilities. Such subtle structure of the many-particle quantum-to-classical transition constitutes the general rule, whereas the monotonicity found in the two-particle case and for bunching events can be considered a rather secluded exception.

Materials and Methods

Distinguishability and Gram–Schmidt Orthonormalization. A photon with arrival time t_i at the BS is described as follows:

$$\mathcal{A}^\dagger_{t_i}|0\rangle = |1_{t_i}\rangle = \int_{-\infty}^{\infty} \mathrm{d}\omega \frac{1}{\sqrt{\pi}\Delta\omega} \mathrm{e}^{-\frac{(\omega-\omega_0)^2}{2\Delta\omega^2}} \mathrm{e}^{i\omega t_i} \mathcal{A}^\dagger_\omega |0\rangle,$$

where ω_0 is the central frequency, $\Delta\omega$ is the frequency width, and $\mathcal{A}^\dagger_\omega$ creates a photon of frequency ω in an input mode $\mathcal{A}$. The distinguishability of two photons with different arrival times t_1 and t_2 is quantified by their temporal overlap $\alpha = \langle 1_{t_1}|1_{t_2}\rangle$, which results in Eq. **1**. Consequently, the t_2 photon can be decomposed—with respect to its position on the time axis—by orthogonal projection onto one strictly indistinguishable component $\alpha|1_{t_1}\rangle$ and onto one (orthogonal) fully distinguishable component $\sqrt{1-\alpha^2}|\tilde{1}_{t_1}\rangle$, defined as follows:

$$|\tilde{1}_{t_1}\rangle = \frac{|1_{t_2}\rangle - \alpha|1_{t_1}\rangle}{1-\alpha^2}, \qquad [6]$$

such that

$$\mathcal{A}^\dagger_{t_2}|0\rangle = |1_{t_2}\rangle = \left(\alpha\mathcal{A}^\dagger_{t_1} + \sqrt{1-\alpha^2}\mathcal{A}^\dagger_{\tilde{t}_1}\right)|0\rangle = \alpha|1_{t_1}\rangle + \sqrt{1-\alpha^2}|\tilde{1}_{t_1}\rangle. \qquad [7]$$

Because the phase of α is not observable in our setting, we assume $\alpha \in \mathbb{R}$, without loss of generality.

Postselection of Fock States. The quantum state of the photons, prepared by the spontaneous parametric downconversion (SPDC) process, at the input modes of the BS is given as $\sum_{j=0}^{\infty}\eta^j|j,j\rangle_{ab}$, where $|\eta|^2$ is the probability for photon pair generation. The photon distribution at the output modes of the BS is measured using the setup shown in Fig. 1*B*. For the SPDC process in our experiment, $|\eta|^2$ is <0.01, which makes the contribution of $|n,n\rangle_{ab}$ dominant over the contributions of $|j,j\rangle_{ab}$ for $j > n$. Therefore, although the single-photon detectors used in this experiment are not number resolving, coincidence measurement of two and four detectors at the output modes of the BS can effectively postselect the quantum state at the input mode $|1,1\rangle_{ab}$ and $|2,2\rangle_{ab}$, respectively. Photon loss in the interferometer and less-than-unity detection efficiency simply affects the overall coincidence count rates because only successful events are recorded and contributions from the $|j,j\rangle_{ab}$ terms for $j \geq 3$ are negligible compared with that from $|1,1\rangle_{ab}$ and $|2,2\rangle_{ab}$ in our experiment.

Experimental Setup. A multiphoton quantum state is generated via the noncollinear frequency-degenerate SPDC process at a 2-mm-thick β-barium-borate (BBO) crystal pumped by a femtosecond laser pulse (central wavelength, 390 nm; average power, 120 mW), which is focused onto the BBO crystal by a lens of 300-mm focal length. The generated photons are centered at 780 nm and filtered by interference filters of 4-nm FWHM. The photons are coupled into two single-mode fibers located at a distance of 430 mm from the BBO, where each fiber corresponds to an input mode (*a*, *b*) in Fig. 1*A*. The twofold coincidence count rate observed with single-photon counting detectors (Perkin-Elmer SPCM-AQ4C) directly coupled to the fiber is ∼13 kHz. The coincidence circuit has an 8-ns coincidence window. At each output of the fiber, a half-wave plate and a quarter-wave plate adjust the polarization state of the photon and a motorized stage connected to the fiber tip at the mode *b* changes the path delay *x*. After the BS, photons are coupled into single-mode fibers, which are then directly connected to single-photon counting detectors as shown in Fig. 1*B*.

ACKNOWLEDGMENTS. Financial support by the National Research Foundation of Korea (2011-0021452 and 2012-002588), through Deutscher Akademischer Austausch Dienst/German–Korean Partnership Program Grant D/09/02090, and by the German National Academic Foundation (M.C.T.) is gratefully acknowledged. H.-T.L. acknowledges support from National Junior Research Fellowship Grant 2012-000642.

1. Grangier P, Roger G, Aspect A (1986) Experimental evidence for a photon anticorrelation effect on a beam splitter: A new light on single-photon interferences. *Europhys Lett* 1(4):173–179.
2. Gerlich S, et al. (2011) Quantum interference of large organic molecules. *Nat Commun* 2:263.
3. Englert BG (1996) Fringe visibility and which-way information: An inequality. *Phys Rev Lett* 77(11):2154–2157.
4. Buchleitner A, Hornberger K, eds (2002) *Coherent Evolution in Noisy Environments* (Springer, Berlin).
5. Arndt M, Buchleitner A, Mantegna RN, Walther H (1991) Experimental study of quantum and classical limits in microwave ionization of rubidium Rydberg atoms. *Phys Rev Lett* 67(18):2435–2438.
6. Steck DA, Milner V, Oskay WH, Raizen MG (2000) Quantitative study of amplitude noise effects on dynamical localization. *Phys Rev E* 62(3):3461–3475.
7. Carvalho ARR, Mintert F, Buchleitner A (2004) Decoherence and multipartite entanglement. *Phys Rev Lett* 93(23):230501.
8. Dür W, Briegel HJ (2004) Stability of macroscopic entanglement under decoherence. *Phys Rev Lett* 92(18):180403.
9. Konrad T, et al. (2008) Evolution equation for quantum entanglement. *Nat Phys* 4(2):99–102.
10. Almeida MP, et al. (2007) Environment-induced sudden death of entanglement. *Science* 316(5824):579–582.
11. Schrödinger E (1935) Die gegenwärtige Situation in der Quantenmechanik. *Naturwissenschaften* 23(48):807–812.
12. Peruzzo A, Laing A, Politi A, Rudolph T, O'Brien JL (2011) Multimode quantum interference of photons in multiport integrated devices. *Nat Commun* 2:224.
13. Hong CK, Ou ZY, Mandel L (1987) Measurement of subpicosecond time intervals between two photons by interference. *Phys Rev Lett* 59(18):2044–2046.
14. Pittman TB, et al. (1996) Can two-photon interference be considered the interference of two photons? *Phys Rev Lett* 77(10):1917–1920.
15. Xiang GY, et al. (2006) Demonstration of temporal distinguishability in a four-photon state and a six-photon state. *Phys Rev Lett* 97(2):023604.
16. Chen L, Li CF, Gong M, Sun FW, Guo GC (2009) A new analysis of multi-photon interference. *Europhys Lett* 85(1):14001.
17. Ou ZY, Rhee JK, Wang LJ (1999) Observation of four-photon interference with a beam splitter by pulsed parametric down-conversion. *Phys Rev Lett* 83(5):959–962.
18. Niu XL, et al. (2009) Observation of a generalized bunching effect of six photons. *Opt Lett* 34(9):1297–1299.
19. Tichy MC, et al. (2011) Four-photon indistinguishability transition. *Phys Rev A* 83(6):062111.
20. Kwiat PG, Waks E, White AG, Appelbaum I, Eberhard PH (1999) Ultrabright source of polarization-entangled photons. *Phys Rev A* 60(2):R773–R776.
21. Kwiat PG, Berglund AJ, Altepeter JB, White AG (2000) Experimental verification of decoherence-free subspaces. *Science* 290(5491):498–501.
22. Kokorowski DA, Cronin AD, Roberts TD, Pritchard DE (2001) From single- to multiple-photon decoherence in an atom interferometer. *Phys Rev Lett* 86(11):2191–2195.

23. Legero T, Wilk T, Hennrich M, Rempe G, Kuhn A (2004) Quantum beat of two single photons. *Phys Rev Lett* 93(7):070503.
24. Legero T, Wilk T, Kuhn A, Rempe G (2006) Characterization of single photons using two-photon interference. *Adv At Mol Opt Phys* 53:253–289.
25. Tichy MC (2011) Entanglement and interference of identical particles. PhD thesis (Albert-Ludwigs-Universität, Freiburg, Germany).
26. Laloë F, Mullin WJ (2012) Quantum properties of a single beam splitter. *Found Phys* 42(1):53–67.
27. Kim YH (2003) Measurement of one-photon and two-photon wave packets in spontaneous parametric downconversion. *J Opt Soc Am B* 20(9):1959–1966.
28. Tichy MC, Tiersch M, de Melo F, Mintert F, Buchleitner A (2010) Zero-transmission law for multiport beam splitters. *Phys Rev Lett* 104(22):220405.
29. Liu BH, et al. (2007) Demonstration of controllable temporal distinguishability in a three-photon state. *Europhys Lett* 77(2):24003.
30. Gurian JH, et al. (2012) Observation of a resonant four-body interaction in cold cesium Rydberg atoms. *Phys Rev Lett* 108(2):023005.